Controls on subtropical low cloud as diagnosed from AIRS, MODIS, and ECMWF-interim reanalysis and the inferred changes low cloud fraction in a warming climate

Daniel T. McCoy[1]*, Ryan Eastman[1], Dennis L. Hartmann[1], Robert Wood[1]

* dtmccoy@atmos.uw.edu

[1] Atmospheric Sciences Department, University of Washington, Seattle, USA

Abstract:

Decreases in subtropical low cloud cover (LCC) occur in climate model simulations of global warming. In this study the observational data records from Moderate Resolution Spectroradiometer (MODIS) and Atmospheric Infrared Sounder (AIRS) spanning 2002-2014 are combined with European Centre for Medium-Range Weather Forecasts (ECMWF) interim reanalysis to compute the dependence of the observed variability of LCC on various predictor variables. Large-scale thermodynamic and dynamical predictors of LCC are selected based on insight from large-eddy simulations (LES) and observational analysis. The observational record from AIRS, MODIS, and ECMWF-interim is used to diagnose how LCC is dependent on each predictor. It is found that increasing inversion strength is associated with increased LCC. Drying of the free-troposphere is associated with decreased LCC. Decreased LCC accompanies subsidence. Finally, it is found that increasing SST leads to a decrease in LCC. This behavior is particularly strong in the trade-cumuli dominated sub-tropics. Based upon the observed response of low cloud to natural variability of the control parameters, we estimate the change in LCC for an idealized, uniform 1K increase in SST and the CMIP5-projected concomitant changes in estimated inversion strength (EIS), free tropospheric relative humidity, and subsidence. LCC is inferred to decrease by 2-3% K^{-1} across the subtropics

if the ocean is warmed uniformly. The reduction in LCC with warming predicted by this method suggests a larger decrease in subtropical cloud cover than predicted by climate models.

1. Introduction:

Oceanic boundary layer cloud cover strongly affects reflected shortwave (SW) radiation and has relatively little effect on the outgoing longwave (LW), leading to a negative cloud radiative effect that significantly impacts the Earth's radiative balance [*Hartmann and Short*, 1980]. The overall response of low clouds to warming is highly uncertain [*Bony et al*., 2006; *Caldwell et al*., 2013; *Vial et al*., 2013; *Webb et al*., 2013]. Despite this uncertainty, a recurrent feature of global climate models (GCMs) is a positive shortwave (SW) cloud feedback across the subtropics due to a decrease in boundary layer cloud cover, however the strength of this decrease varies greatly across the model ensemble [*Zelinka et al*., 2012; *Zelinka et al*., 2013]. Ultimately, this uncertainty in the cloud feedback leads to significant uncertainty in the equilibrium climate sensitivity (ECS) [*Vial et al*., 2013; *Webb et al*., 2006].

Because clouds depend on turbulent motions with a scale much smaller than the GCM horizontal resolution, GCMs must assume that low cloud cover (LCC) is dependent on large-scale thermodynamic and dynamic parameters [*Qu et al*., 2014a; *Qu et al*., 2015; *Quaas*, 2012]. Here we quantify the observed dependence of subtropical cloud cover on various large-scale predictors using multiple linear regression analysis of the record afforded to us by remote sensing and reanalysis. Our study corroborates the results of *Myers and Norris* [2014], who investigated the dependence of SW cloud radiative effect (CRE) and cloud fraction anomalies on meteorological predictor variables in the context

of total derivatives. We also corroborate the results presented in *Qu et al*. [2015], who analyzed inter-annual variability in LCC in the stratocumulus regimes in both GCMs and observations.

In section 2 we will detail the remote sensing and reanalysis datasets used in this study. In section 3 the dependence of low cloud cover (LCC) on large-scale predictors is evaluated. Section 4 discusses the ability of these predictors to reproduce the observational record of LCC across the subtropics. Finally, section 5 offers an estimate of the change in LCC inferred from the observational record of LCC and changes in thermodynamic and dynamic predictors consistent with an idealized warming of the sea surface. These estimates are compared to the model projected change in total cloud cover.

2 Methods:

2a Data:

We consider two different data sets to investigate low cloud dependence on various predictors. These methods may be considered in a Bayesian sense as: (1) $P(L)$, the probability of low cloud irrespective of higher cloud presence, and (2) $P(L|Liquid \wedge SingleLayer)$, the probability of detecting low cloud given that the cloud is single-layered and liquid-topped. In the former case a random overlap is assumed. In the latter case no assumptions are made regarding overlap, although the data is a restricted subset. Each cloud fraction retrieval is paired with relevant collocated thermodynamic and dynamic properties. The analysis is carried out in the latitude band 40°S-40°N. In this study we will use both data averaged over 8-day periods and instantaneously retrieved data. Both probabilities are daytime only. It is important to note

that the purpose of this comparison is not to evaluate time-scale dependencies of various predictors. The data sets used for the 8-Day and 1-Day timescales are too different to offer a clean comparison. We have selected data from these averaging periods to show that the results of our analysis are qualitatively insensitive to the manner used to measure LCC. We will now discuss each data set.

2b MODIS:

Moderate Resolution Spectroradiometer (MODIS) instruments ride aboard both the Terra and Aqua platforms [*Oreopoulos*, 2005; *Platnick et al*., 2003]. We will use this instrument to study the dependence of cloud fraction on large-scale control variables during 2002-2014. We consider two different approaches to describing the prevalence of low cloud. First, we consider low cloud assuming that clouds are randomly overlapped i.e. $P(L)$ as discussed above. Active remote-sensing indicates that random overlap is a reasonable assumption outside of regions of deep convection and land masses [*Li et al*., 2015; *McCoy et al*., 2014]. To calculate P(L) we use the 8-Day averaged MODIS CTP histogram from the Aqua collection 6 data set filtered for sensor zenith angles of less than 32°, which reduces bias in cloud fraction retrieval [*Maddux et al*., 2010]. We will refer to this time resolution as *8-Day*. Low clouds are defined to be CTP>680hPa. Second, we use instantaneous cloud fraction retrievals from the Aqua collection 5.1 data filtered to only include scenes where the cloud is all liquid-topped and single-layered i.e. $P(Cloud|Liquid \wedge Single\ Layer)$. This time resolution will be referred to as *1-Day*. All data sets are gridded to 1° resolution. We will now discuss the collocated thermodynamic

and dynamic data sets pertaining to each of these cloud fraction retrievals. These are also summarized in Table 1.

2c AIRS:

The Atmospheric Infrared Sounder (AIRS) rides aboard the Aqua and Terra platforms. It is a grating infrared spectrometer, which provides a vertical profile of atmospheric thermodynamic properties [*Aumann et al*., 2003]. In this study we will be using the 8-Day averaged data from the AIRS collection 6 to describe free tropospheric relative humidity in combination with 8-Day cloud fraction data from MODIS. Relevant properties from AIRS are used to calculate EIS[*Wood and Bretherton*, 2006], and supplementary analysis is performed using the AIRS-predicted near surface RH and air temperature.

2d ECMWF-Interim:

In this study we use data from the European Centre for Medium-Range Weather Forecasts (ECMWF) interim reanalysis (ECMWF-Interim) [*Dee et al*., 2011] to examine several thermodynamic and dynamic predictors. The 4-times daily output from ERA-Interim is interpolated to the local overpass time for the Aqua satellite. Thermodynamic predictor variables are used in conjunction with the 1-Day cloud fraction data set. The 10-meter wind speed (U10m) and pressure velocity at 550 hPa ($\omega 550$) are used in conjunction both the 1-Day and 8-Day data sets because no equivalent dynamical retrieval product is available from AIRS.

2e Compositing analysis:

LCC exhibits considerable spatial variability across the subtropical oceans (Figure 1). Although macrophysical and microphysical factors determine the coverage of low cloud [*Albrecht*, 1989; *Nakajima et al*., 2001], in this study we consider only the relationship of low cloud to large-scale thermodynamic and dynamic variables. We utilize multiple-linear regression because many of the predictor variables considered in this study are correlated with each other (Figure 2).

We choose several control variables that have been established by previous studies as important drivers of LCC. We will take the observational record from 40°S-40°N, 2002-2014 and composite LCC upon these control variables. To evaluate the robustness of the compositing analysis across different regimes we performed compositing individually on each 20° latitude band between 40°N and 40°S. In each latitude band, compositing was performed individually on each season to reduce the impact of the seasonal cycle of the dependence of LCC on the control variables (January-March, April-June, July-September, and October-December). The same analysis was repeated on the regions identified as stratocumulus dominated by *Klein and Hartmann* [1993], and on the regions dominated by trade cumulus. These regions are shown in Figure 1. This allows us to determine if the dependence of LCC on large-scale control variables is a robust behavior within each cloud regime or if it is a function of transitioning from stratocumulus regimes to trade cumulus regimes [*Eastman et al*., 2011; *Schreier et al*., 2014].

In this investigation we assume that low cloud coverage may be parameterized in terms of large-scale variables. This is problematic because correlation is not causation

and cloud coverage and boundary layer properties affect each other. This issue is common to observational studies of the dependence of low cloud on atmospheric predictors [*Eastman and Wood*, 2015; *Klein and Hartmann*, 1993; *Qu et al*., 2015; *Yue et al*., 2013], and we acknowledge this issue. We provide the following arguments to support the view that the large-scale properties we have chosen have value as control variables. First, we refer to modeling analysis in support of mechanistic linkages between LCC and each predictor variable. Second, while clouds determine the boundary layer properties to some degree, we ameliorate this problem by selecting predictors of boundary layer properties that are somewhat more external to the boundary layer and are not as directly impacted by the cloud cover. That is to say, this work considers SST and wind speed, as opposed to air-temperature and relative humidity within the boundary layer, although it might be argued that the latter variables more directly influence cloud cover. Further, we compare aggregated 8-Day and instantaneous 1-Day data. It seems reasonable to suppose that the effect of cloud cover on large-scale properties will be less pronounced on shorter time scales. All this being said, we cannot completely discount the possibility that relations between large-scale predictors and LCC are correlative, rather than causative. We will now discuss the predictor variables that we consider in this study and their anticipated effect on LCC. We have summarized these variables in Table 1.

Stronger inversions capping the planetary boundary layer (PBL) trap moisture more effectively, enhancing cloud fraction [*Klein and Hartmann*, 1993; *Wood and Bretherton*, 2006] and increasing its persistence [*Eastman and Wood*, 2015]. The importance of lower tropospheric stability (LTS) and, subsequently estimated inversion strength (EIS) has been thoroughly established through numerous observational analyses

[*Klein and Hartmann*, 1993; *Koshiro and Shiotani*, 2014; *Myers and Norris*, 2013; 2014; *Wood and Bretherton*, 2006]. ECMWF-interim and AIRS data describing atmospheric temperature, pressure, and near surface RH and T are used to calculate EIS as detailed in *Wood and Bretherton* [2006]. Near surface properties are estimated at 1000 hPa in the ECMWF-interim data set. A positive correlation between EIS and LCC is expected based on previous observational studies.

Drying of the subtropical free-troposphere has been hypothesized as the driver of the decreasing subtropical LCC predicted in GCMs as the climate warms [*Sherwood et al*., 2014; *Tsushima et al*., 2006]. Modeling and observational studies find that as the subtropical free-troposphere dries, in a relative sense, entrainment of warmer and drier air from the subtropical free-troposphere leads to a thinning of low cloud by increasing the lifting condensation level more than the cloud top height [*Blossey et al*., 2013; *Bretherton et al*., 2013; *Wood*, 2007; 2012], although thickening may occur for deep boundary layers and a free tropospheric RH above 40% [*Randall*, 1984]. Coupling between free-tropospheric humidity and cloudiness is supported by large eddy simulation (LES) and mixed-layer model (MLM) simulation [*Bretherton et al*., 2013; *de Roode et al*., 2014; *van der Dussen et al*., 2015].

LES studies indicate that decreasing subsidence allows cloud to thicken, although this seems to be regime and model dependent [*Blossey et al*., 2013; *Bretherton et al*., 2013]. Observations indicate that EIS and subsidence are often correlated, but multiple linear regression and compositing show that EIS and subsidence have independent effects on LCC and that subsidence tends to reduce LCC at constant EIS [*Myers and Norris*, 2013].

Because boundary layer relative humidity stays almost constant in a warming climate [*Held and Soden*, 2000] early GCMs assumed clouds did not change as the climate warmed and several years passed before cloud feedbacks became part of the scientific literature [*Schneider*, 1972]. Observational analysis of SST and stratiform cloud cover anomalies show a robust negative relationship in the midlatitudes and eastern oceans [*Clement et al*., 2009; *Eastman et al*., 2011; *Klein et al*., 1995; *Kubar et al*., 2012; *Norris and Leovy*, 1994]. Single-column and LES modeling robustly reduces cloudiness with warming in a constant relative humidity setting [*Bretherton and Blossey*, 2014; *Bretherton et al*., 2013; *Brient and Bony*, 2013; *Rieck et al*., 2012]. The mechanisms underlying this change have proven to be somewhat subtle to interpret. Recent LES modeling work has hypothesized a mechanism that could explain this behavior. We will now briefly summarize the enhanced liquid flux (ELF) adjustment mechanism that was described in *Bretherton and Blossey* [2014] to explain the decrease in cloud cover with enhanced SST diagnosed in LES simulations in the context of a fast adjustment to an instantaneous warming. As presented in *Bretherton and Blossey* [2014], this mechanism applies to instances of cumulus-topped and cumulus under stratocumulus.

Consider a cloud-topped turbulent boundary layer with some radiative destabilization at cloud top maintaining the cloud. The SST and liquid water temperature through the boundary layer and inversion are increased uniformly (where liquid water temperature is $T - q_l \times L/c_p$; and where q_l is the cloud liquid water mixing ratio, L is the latent heat of vaporization, and c_p is the specific heat of dry air at constant pressure). The inversion strength is held fixed. The specific humidity is increased so that the relative

humidity remains fixed. The radiative flux divergence at the top of the boundary layer is held constant.

In the context of this explanation of the ELF adjustment mechanism, these changes to the boundary layer properties are made instantaneously. To maintain constant RH, specific humidity will increase by approximately 7%/K, following Clausius-Clapeyron. Within the cloud layer this results in an amplification of the horizontal variations in liquid water. This induces variations in horizontal temperature, and subsequently buoyancy. The liquid water increases by only 2-3%/K because over half of the increase in total specific humidity goes into increasing the saturation mixing ratio (see *Betts and Harshvardhan* [1987]). Ultimately, this perturbation increases the difference between updraft and downdraft liquid water and temperature, resulting in a 2-3%/K increase in buoyancy flux. This enhanced buoyancy flux increases the entrainment of warm, dry air from the free troposphere. The LES simulation responds by drying and warming of the upper portion of the mixed-layer. The updrafts and downdrafts decrease their liquid flux, and ultimately the cloud adjusts so that the cloud thins and the entrainment rate comes into balance with the fixed radiative destabilization at cloud top.

We present this discussion of the ELF adjustment mechanism as a potential physical a-priori to justify the dependence of LCC on SST. Whether the mechanism underlying it is ELF adjustment or not, LES-simulated clouds appear to thin substantially as the SST increases while the relative humidity stays fixed [*Bretherton and Blossey*, 2014; *Rieck et al*., 2012]. Because LES models appear to generally thin cloud cover as SST increases and boundary layer relative humidity stays fixed [*Blossey et al*., 2013; *Bretherton and Blossey*, 2014; *Bretherton et al*., 2013; *Rieck et al*., 2012] we composite

on both the SST and the wind speed. Wind speed enhances the flux of water vapor from the ocean surface into the PBL. Based on the existing LES and SCM studies, we expect LCC to be negatively correlated with SST at a constant wind speed.

3. Results of compositing analysis

For each set of compositing variables shown in Table 1, sixteen composites of LCC were created for the 40°S-40°N region (four 20° latitude bands and four seasons), twenty composites were created in the trade cumulus region (five regions and four seasons), and twenty composites were created in the stratocumulus regions (five regions and four seasons). The trade cumulus and stratocumulus regions are diagramed in Figure 1; latitude markers indicate the remaining four latitude bands. Multiple linear regression was performed on each composite to yield coefficients relating LCC and each predictor variable. The values of these coefficients for each set of predictor variables and for the 1-Day and 8-Day data sets over the latitude bands, and stratocumulus and trade cumulus regimes are shown in Figure 3. For each predictor variable the coefficients are weighted by the standard deviation in time and space of that predictor variable 40°S-40°N and 2002-2014. Coefficients relating each predictor variable to LCC are provided in Table 3. For each region and data set there are several estimates of each regression coefficient from sub-regions and seasons (16 in the trade cumulus, 16 in the stratocumulus, and 20 in the 40°S-40°N latitude bands). The spread and median values of each coefficient are shown in Figure 3.

The latitude-band composite from 40°S-40°N were averaged together over the four seasons to create a global-mean and annual composite. The behavior of the LCC in the global-mean-annual composite was found to be relatively linear. Over 80% of the

variability in LCC in the composite was explained by a multiple linear regression on the predictor variables, indicating that the predictors add relatively linearly. This is consistent with the results of LES modeling [*Bretherton et al*., 2013]. We will now discuss robust features of our analysis that agree between regions, sub-regions, and seasons.

Our analysis shows that EIS and LCC are positively correlated. This is consistent with the results of previous observational studies relating LCC to EIS in the stratocumulus regions that did not control for other predictor variables [*Klein and Hartmann*, 1993; *Koshiro and Shiotani*, 2014; *Wood and Bretherton*, 2006]. We find that the dependence of LCC on EIS varies between regions and data sets (Table 3). The relation between EIS diagnosed in the stratocumulus regions varies between 10.6%/K and 2.0%/K for the 1-Day and 8-Day data sets, respectively. This range encompasses the estimates yielded by observations of 6%/K [*Wood and Bretherton*, 2006], 2-3.5%/K [*Qu et al*., 2015], and 5.3%/K [*Koshiro and Shiotani*, 2014]. The estimate for the 40°S-40°N region as a whole is between 9.5%/K (1-Day) and 4.2%/K (8-Day). This agrees qualitatively with *Koshiro and Shiotani* [2014], who diagnosed a relationship between LCC and EIS of 4.7%/K using ship-based observations over the 60°S-60°N region, and with *Myers and Norris* [2013], who used satellite observations between 30°S-30°N to estimate a LCC-EIS relationship of 4.0-4.9%/K, depending on dataset.

Wind speed is found to positively correlate with LCC, which is also consistent with expectations from LES modeling [*Bretherton et al*., 2013]. SST is found to be strongly negatively correlated with LCC, which is consistent with both modeling and observational studies [*Bretherton and Blossey*, 2014; *Myers and Norris*, 2014; *Norris and Leovy*, 1994; *Qu et al*., 2015]. In keeping with previous studies [*Myers and Norris*, 2014;

Qu et al., 2015], the relation between SST and LCC is both the most influential of the predictor variables and the most uncertain (Figure 3). Positive correlation between wind speed and LCC is consistent with the enhancement of the moisture flux into the boundary layer. The negative correlation between SST and LCC is consistent with previous observational and modeling studies [*Bretherton and Blossey*, 2014; *Brient and Bony*, 2013; *Myers and Norris*, 2014; *Qu et al*., 2015]. The correlation between SST and LCC is only found to be weakly and uncertainly positive in the in the stratiform regions and in the global composite in the 1-Day data set. The source of the disagreement between the LCC dependence on SST between the 1-Day and 8-Day data sets in the stratiform regions is unclear, especially because the data sets being used are fundamentally different in the way that they interpret LCC. One possible explanation is that the lag between SST and boundary layer temperature manifests more strongly in the relatively small stratiform region in the instantaneous (1-Day) data set, or it may simply be due to the much smaller data volume included in the stratocumulus regions as compared to the trade cumulus regions (see Figure 1). While the argument that the predictors describe a causal linkage is weaker, it is interesting to contrast these results to the same analysis performed using near-surface air temperature and relative humidity instead of SST and U10m. The near-surface air temperature and RH are predicted in the collection 6 AIRS data and are used in conjunction with the 8-Day data set. ECMWF-interim is used for the 1-Day data. When the analysis is repeated using RH and T in the boundary layer as predictors the uncertainty in the dependence of LCC on near surface air temperature (Figure 4) is much smaller than the uncertainty in the dependence of LCC on SST (Figure 3). The sign of the dependence is also consistent between the trade cumulus regions and stratocumulus

regions (Figure 4). This is consistent with a time lag between SST and air temperature. Ultimately, the disagreement between the stratocumulus regions and the rest of the subtropics regarding the relation between SST and LCC does not significantly affect the overall dependence of LCC on SST inferred from the global data, and does not significantly affect the inferred change in LCC consistent with an increase in SST. The inferred change in LCC due to an increase in SST and accompanying changes to other predictors is discussed in section 5.

Relative humidity in the free-troposphere was found to positively correlate with LCC, consistent with expectations from LES and observations [*Bretherton et al*., 2013; *Myers and Norris*, 2014]. Finally, subsidence was found to have a weak negative correlation with LCC with the exception of the 8-Day data in the stratocumulus regions. A negative correlation between subsidence and LCC is consistent with the results of LES simulations [*Blossey et al*., 2013; *Bretherton and Blossey*, 2014; *Bretherton et al*., 2013] and observational analysis [*Myers and Norris*, 2013; *Qu et al*., 2015].

The relation between predictor variables and LCC remain qualitatively the same with the exception of the SST dependence diagnosed by the 1-Day data in the stratocumulus regions. This is particularly interesting because the way that LCC is represented differs substantially between the 1-Day and 8-Day data sets. The 1-Day LCC represents an instantaneous retrieval and no assumptions about overlap are made, while the 8-Day data set aggregates a large number of observations together assuming the cloud cover is randomly overlapped. It is also worth noting that the relations between predictor variables and LCC are qualitatively consistent with the expectations in the literature regarding subtropical marine low cloud. The estimated dependence of LCC on SST and

EIS presented in *Qu et al*. [2015] as derived from inter-annual anomalies in the stratocumulus regions is between -0.9%/K to -3.8%/K and 2.0%/K to 3.5%/K, respectively. This is a much weaker dependence on EIS than diagnosed by the 1-Day data set (10.6±4.0%/K), but is closer to the estimate offered by the 8-Day data (2.0±2.4%/K). Regression of LCC on SST in the stratocumulus regions is not robust in the 1-Day data set (5.5±18.0%/K), or in the 8-Day data set (-0.9±10.3). It is interesting to note that the SST dependence diagnosed from the stratocumulus regions in our study is considerably less robust than the SST dependence in the trade cumulus regions (see Table 3). This suggests that the dependence of LCC on SST in GCMs should be considered separately in each region to quantify their decrease in cloud fraction in a warming climate. Given the current methodology by which information on cloud fraction is archived for the bulk of GCMs, the dependence of LCC on SST studies such as *Qu et al*. [2014a] and *Qu et al*. [2015] must focus on the stratocumulus regions where low clouds remain relatively un-obscured by overlying cloud and the GCM-archived cloud fraction available for the coupled model intercomparison project (CMIP) may be used as a measure of LCC. Based on our results we recommend that studies compare and contrast the stratocumulus and trade wind cumulus regions utilizing satellite simulators in GCMs (see *Bodas-Salcedo et al*. [2011]). The current generation of GCMs in CMIP5 has only implemented satellite simulators in a few models, making evaluation of the multi-model LCC dependence problematic.

4 Reproduction of LCC from observed large-scale predictors

Now that we have examined the historical record and have diagnosed the dependence of LCC on various predictors, we wish to evaluate how much of the observed variability in LCC may be reproduced using these dependencies. We re-grid the data sets to 4°x4° monthly resolution. The mean composite created by averaging the 16 composites form 40°S-40°N is used to predict the historical LCC based on the historical predictor variables. The observed historical LCC and the LCC predicted by this method are compared. The predicted LCC reproduces over 49% of the variance in observed historical LCC when the coefficients from the multiple linear regression are used and over 54% of the variance in historical LCC if the composited LCC is used as a look up table. Within the look up table, missing values (compositing bins where less than 50 observations exist in the observational record) are extrapolated using penalized least squares [*Garcia*, 2010; *Wang et al*., 2012] (see Table 2 for the R^2 for the LCC predicted by multiple linear regression and by the look up table).

The ability of the predictor variables to reproduce the observed time series of LCC at each point is evaluated in Figure 5. As before, the LCC is predicted for both the 1-Day and 8-Day data sets using the mean composite created using data from the 40°S-40°N region first used as a look up table and then using the coefficients for each predictor variable as derived from the mean composite (Table 3). The predicted LCC and observed LCC for both data sets are averaged to 4°x4° monthly resolution and the correlation is evaluated at each latitude and longitude grid point (Figure 5, second and fourth rows).

The seasonal cycle provides a significant fraction of the local variability in LCC in many regions. To more rigorously evaluate the prediction of LCC the climatological seasonal cycle is removed from each grid point and the correlation between anomalies is

calculated. Both 8-Day and 1-Day data sets show significant correlations between the observed time series of LCC in most regions (Figure 5, first and third rows). Significant positive correlations between predicted anomalies and observed anomalies exists in both data sets, although the correlations appear to be somewhat more positive in the case of the 1-Day data set (Figure 5, first and third rows of the left column). Negative correlations between predicted and observed LCC time series in the 8-Day dataset occur in the Canarian (15°N-25°N and 25°W-35°W) and, to a lesser extent, the Californian (20°N-30°N and 120°W-130°W) stratocumulus regions.

It is interesting to evaluate the impact of variability in each predictor variable on LCC. The coefficients yielded by multiple linear regression performed on the mean composite are used to calculate LCC. The variance contributed by each term in the multiple linear regression model

$$LCC = a_1 \times EIS + a_2 \times U10m + a_3 \times w550 + a_4 \times SST + + a_5 \times RHFT \qquad [1]$$

is calculated and scaled by the total predicted variance in LCC. The fractional variance of each term in the 1-Day and 8-Day data sets is shown in Figure 6. EIS contributes more of the variance in the 8-Day data set than in the 1-Day data set. In both data sets the variance in EIS is centered over the stratocumulus regimes. Wind speed also appears to contribute more strongly to variability in the 8-Day data set over the tropics than in the 1-Day data set. It should be noted that the variance shown in Figure 6 contains both seasonal and inter-seasonal variability. The intention of this figure is to show the variance in LCC that is contributed by each predictor variable. For instance, a great deal of the

variance in LCC over the stratocumulus regimes is contributed by EIS, as one would expect from previous studies of the seasonal dependence of LCC on EIS in these regions [*Klein and Hartmann*, 1993; *Wood and Bretherton*, 2006].

Variability in subsidence and free tropospheric RH both contribute more strongly to variability in LCC in the 1-Day data set than in the 8-Day data set with contributions centered over the regions of large-scale ascent where subsidence and RHFT are both highly variable. Finally, variance in SST contributes much more strongly in the 8-Day data set. Overall, a considerable amount of the variability in the current climate is due to EIS, wind speed, and SST, with subsidence and free tropospheric RH playing relatively localized roles. It must be noted that a large contribution to the variance in the current climate does not necessarily equate to a large contribution to the change in LCC in a warming climate. We will now discuss the systematic change in all of these variables projected in a warming climate and the inferred change in LCC.

5 Change in LCC in a warming climate inferred from observed variability

Given that we are able to predict observed variability in LCC using the compositing technique described above (Figure 5), we now investigate how LCC might change in a warmed climate if LCC in a warmed climate depends on the predictor variables we have chosen in the same way it does in the current climate.

Naturally, this somewhat oversimplifies matters. Atmospheric emissivity will be increased by greenhouse gases (GHGs). This suppresses cloud top cooling and is likely to thin clouds [*Bretherton et al.*, 2013]. We do not have a good methodology to probe this dependence in the current climate and we neglect it from our analysis, noting that LCC is

likely to be decreased by enhanced GHGs in addition to the effects of changing the predictors considered here. Aerosol effects on cloud fraction remain highly uncertain and are not investigated here.

To estimate the changes in LCC consistent with a uniform 1K ocean warming we assume that SST increases by 1K everywhere. Wind speed is assumed to not change. It is worth noting that observations and modeling studies indicate localized increases and decreases in surface wind speed, although the global change is uncertain [*Richter and Xie*, 2008; *Zieger et al*., 2014]. For the sake of simplicity we consider wind speed to be constant with warming in the present analysis. It should be noted that the regression coefficient relating the LCC and U10m is relatively large: 3.6±1.1 %s/m in the 8-Day data set and 6.0±1.5 %s/m in the 1-Day data set. The minimum observed trend in surface wind speed in the subtropics is -0.8 $ms^{-1}K^{-1}$ and areas with substantial positive trends may exceed 1 $ms^{-1}K^{-1}$[*Zieger et al*., 2014]. This implies that significant local increases and decreases in LCC due to changing wind speed are possible. EIS is assumed to change by 0.2K per degree of surface warming, consistent with the mean CMIP5 response to warming [*Webb et al*., 2013] and the forcing used in previous idealized studies [*Bretherton et al*., 2013]. It should be noted that this simplifies the EIS response to warming because GCMs produce significant spatial variability in the change in EIS when the ocean is warmed uniformly [*Qu et al*., 2014b]. We have chosen to use a uniform increase in EIS consistent with the estimate shown in *Webb et al*. [2013] of 0.2K per degree SST increase. It should be noted *Qu et al*. [2014b] found that the largest local increase in the multi-model mean GCM EIS response was less than 1K K^{-1}. Finally, we utilize the multi-model mean change in RHFT and $\omega 550$, normalized by the change in

surface temperature, between the historical and RCP8.5 simulations. The fractional change in $\omega 550$ and RHFT are calculated and are used to scale the observational record to estimate how much RHFT and $\omega 550$ would change due to a degree of surface warming. In the multi-model mean RHFT is estimated to decrease by 1% of its historical value in the subtropics (i.e. $RH_{warm}=0.99*RH_{historical}$) and increase by 5% at the equator. Pressure velocity at 550hPa is estimated to decrease by 2% of its historical value in the subtropics and increases by 4% of its historical value at the equator. The CMIP5 models used are listed in the supplementary material.

The observations of each predictor variable are altered as described above to be consistent with a hypothetical, idealized warmed climate. The mean of the composites from the 40°S-40°N region and the mean of the composites from the trade cumulus regions are separately used as look up tables to predict LCC. The difference between the historical and warmed climate predictions is used to diagnose the change in LCC.

LCC is predicted to decrease by 2-3% (Figure 7 and Figure 8). EIS increases enhance LCC, but these increases are much smaller than the inferred decrease in LCC due to increased SST (Figure 8). Changes in LCC due to the changes in RHFT and subsidence are relatively small (Figure 8). The change in LCC tends to be strongest over the subtropics (Figure 7 and Figure 8). It is interesting to note that while the inferred change in LCC varies depending on which region the data used to create the composites originates from, the predicted change in LCC is relatively robust in terms of sign and magnitude (Figure 8).

While many GCMs decrease subtropical cloud cover in response to warming, the change in LCC that we estimate is more negative than the decrease in total cloud fraction

calculated by 30 GCMs within CMIP5 (Figure 7 and Figure 8, see the supplementary material for a list of GCMs). The change in total cloud fraction in CMIP5 was calculated as the difference between the historical and RCP8.5 simulations scaled by change in SST. The multi-model mean reduction in zonal mean cloud cover in the CMIP5 models is only robustly negative south of 30°S in the southern subtropics (Figure 8). The multi-model mean change in total cloud cover appears to be positive equatorward of 30°S due to strong increases in stratocumulus cloud in some models. Overall, cloud cover decreases in the trade cumulus regions (Figure 7). There is a considerable range in the changes in cloud fraction predicted by the GCMs as can be seen comparing the two outlier models from the ensemble (Figure 7b and Figure 7c). The comparison of our observationally-predicted change in LCC and the change in total cloud cover predicted by CMIP5 models is interesting, but several caveats must be stated that could cause the LCC change predicted here to be biased low or high relative to the change in CMIP5 LCC suggested by the change in total CF. First, GCM total cloud fraction is not equivalent to low cloud fraction [*Bodas-Salcedo et al*., 2011; *Caldwell et al*., 2013]. For instance, total cloud fraction changes might be biased by upper-level cloud obscuring changes in LCC. Second, as noted before, the effects of a more emissive GHG-rich atmosphere have been neglected in this study, which should make the decrease in CF in CMIP5 stronger in models that incorporate these effects [*Qu et al*., 2014a]. Neglecting enhanced atmospheric emissivity from GHGs should make our predicted decrease in LCC conservative relative to GCMs because it does not include this effect. Although both of these biases might be quite significant, it is worth considering that the decrease in LCC that we predict using the observational record is stronger than the change in total cloud

fraction predicted by almost all the GCMs (Figure 7). It seems unlikely that all of this difference is due to either increases in upper-level cloud cover or upper level cloud cover obscuring decreases in LCC. Overall, we find that the enhancement in SST, which is thought to drive the ELF adjustment, contributes very strongly to the decrease in LCC in the subtropics (Figure 8). As discussed in Section 3, an important caveat of this analysis is the influence of LCC on boundary layer and sea surface temperature. LCC will cool the boundary layer and some of the diagnosed dependence of LCC on SST may be due to the effects of LCC on SST. This limitation is inherent in observational analysis of cloud cover. Simulations of PBL cloud where SST is not responsive to cloud cover have shown substantial decreases in LCC with warming [*Bretherton and Blossey*, 2014; *Bretherton et al*., 2013; *Rieck et al*., 2012]. For example, *Bretherton and Blossey* [2014] found cloud liquid water path (LWP) to be halved in one LES study when SST was increased by 4K. Overall, our analysis; previous observational [*Clement et al*., 2009; *Eastman et al*., 2011; *Kubar et al*., 2012; *Myers and Norris*, 2014; *Norris and Leovy*, 1994; *Qu et al*., 2015]; and LES modeling studies [*Blossey et al*., 2013; *Bretherton and Blossey*, 2014; *Bretherton et al*., 2013; *Rieck et al*., 2012] agree in supporting a negative dependence of LCC on SST. Our predicted change in LCC based on observations of current variability suggests that GCMs may not decrease their LCC sufficiently in response to warming.

6 Conclusions

The dependence of LCC on various control variables is examined using the observational record spanning 2002-2014 from AIRS, MODIS, and ERA-interim. Both instantaneous observations of low cloud cover (LCC) and data aggregated over 8-day

periods are used to diagnose the dependence of LCC on EIS, wind speed, SST, free tropospheric RH, and subsidence. The results from these two separate analyses are qualitatively similar. More than 49% of the variance in the observational record of LCC from 2002-2014 and 40°S-40°N over oceans is explained by multiple linear regression on the aforementioned control variables (Table 2). Finally, the change in LCC that is consistent with a 1K SST warming and accompanying changes to other control variables predicted by CMIP5 is estimated, assuming that the dependence of LCC on these control variables is invariant under climate change. We will now discuss the salient points of our analysis. It should be noted that the dependence of LCC on each control variable is discussed in the context of a multiple linear regression, as opposed to a regression on each variable individually.

- EIS is correlated with enhanced LCC, consistent with many previous observational studies [*Klein and Hartmann*, 1993; *Wood and Bretherton*, 2006]. The relation between cloud cover and EIS diagnosed in the stratocumulus regions varies between 10.6%/K and 2.0%/K for the 1-Day and 8-Day data sets, respectively. This range encompasses the estimates from ship-based observations of 6.0%/K [*Wood and Bretherton*, 2006] and 5.3%/K [*Koshiro and Shiotani*, 2014]; and from remote sensing observations of 2.0-3.5%/K [*Qu et al.*, 2015]. We estimate the slope of the EIS-LCC relation for the 40°S-40°N region as a whole as between 9.5%/K (1-Day) and 4.2%/K (8-Day). This agrees qualitatively with *Koshiro and Shiotani* [2014], which diagnosed a relationship between LCC and EIS using ship observations over the 60°S-60°N region of 4.7%/K, and with

Myers and Norris [2013], who used satellite observations between 30°S-30°N to estimate a LCC-EIS relationship of 4.0-4.9%/K.

- Free tropospheric RH is correlated with enhanced LCC, consistent with previous observational and modeling studies [*Bretherton et al*., 2013; *Myers and Norris*, 2014; *van der Dussen*, 2014; *van der Dussen et al*., 2013]. The effects of changes in free tropospheric RH seem to not affect the change LCC in a warming climate.
- Subsidence is correlated with decreased LCC, consistent with other observational [*Myers and Norris*, 2013] and modeling studies [*Blossey et al*., 2013; *Bretherton et al*., 2013]. It should be noted that the change in subsidence inferred from CMIP5 did not significantly change the predicted decrease of LCC in a warming climate.
- Increased wind speed is correlated with enhanced LCC, consistent with previous modeling studies [*Bretherton et al*., 2013].
- SST is correlated with decreased LCC. This effect was found to be particularly strong and is consistent with the decline in LCC as SST rises that is simulated in LES models, and SCMs [*Bretherton and Blossey*, 2014; *Brient and Bony*, 2013; *Rieck et al*., 2012]. A negative correlation with SST is consistent with observational analysis [*Clement et al*., 2009; *Kubar et al*., 2012; *Myers and Norris*, 2014; *Norris and Leovy*, 1994; *Qu et al*., 2015] and GCM behavior [*Brient and Bony*, 2013; *Qu et al*., 2014a; *Qu et al*., 2015]. The dependence of LCC on SST is found to be dependent on regime, with strongly negative relations found in the trade cumulus regions, while there is no clear dependence in the stratocumulus regimes. This disagreement may be due to the timescale linking SST to boundary

layer properties. When SST and U10m are replaced with temperature and RH near the surface the dependence of LCC on near-surface temperature is found to be negative in all regimes.

- A simplified set of changes to the control variables is used to infer the change in LCC consistent with a 1K change in SST and expected concomitant changes in EIS, RHFT, and subsidence estimated by GCMs. Both the 1-Day and 8-Day data sets indicate a decrease in LCC with warming. The 1-Day data set inferred a 2% decrease, while the 8-Day data set inferred a 3% decrease. The majority of this decrease in both data sets is found to be due to SST increases indicating the importance of constraining the SST-LCC relationship in both observations and GCMs.

Overall, it appears that the decrease in subtropical cloud fraction in CMIP5 GCMs[*Qu et al*., 2015; *Zelinka et al*., 2012; *Zelinka et al*., 2013] is qualitatively consistent with the observed dependence of cloud fraction on the various thermodynamic and dynamic controls on LCC shown here. The decrease in total cloud fraction in GCMs is weaker than the predicted change diagnosed here. While this might be because high cloud cover changes in the GCM are occluding the changes in LCC, it is hard to believe that the significant disagreement between our observationally predicted LCC decrease and the GCM-simulated decrease in total cloud is all due to overlying high cloud.

We find that the dependence on SST, which is thought to drive the ELF adjustment mechanism [*Bretherton and Blossey*, 2014], plays a key role in the estimated change in LCC in a warming climate. This is consistent with *Myers and*

Norris [2014], who found that GCMs replicate a decrease in SW CRE with higher SSTs, but underrepresent it relative to the observed dependence. We are also in agreement with the analysis performed by *Qu et al*. [2015], who found a negative correlation between LCC and SST over the stratocumulus regions. Overall, based on the results of this study and previous studies [*Myers and Norris*, 2014; *Qu et al*., 2015], it seems very likely that subtropical LCC will decrease in a warming climate. We also hypothesize that the decrease in LCC, and subsequent positive cloud amount feedback in GCMs is underrepresented. Accurate representation of this effect in GCMs will be important to offering an accurate estimate of climate sensitivity.

Acknowledgements

The authors would like to thank Peter Blossey and Christopher Bretherton for their guidance and advice. D.T.M. and D.L.H. were supported under NASA Grant NNX14AG26G. R.E. and R.W. were supported under NASA grant NNXBAQ35G.

References

Albrecht, B. A. (1989), AEROSOLS, CLOUD MICROPHYSICS, AND FRACTIONAL CLOUDINESS, *Science*, *245*(4923), 1227-1230.

Aumann, H. H., et al. (2003), AIRS/AMSU/HSB on the aqua mission: Design, science objectives, data products, and processing systems, *Ieee Transactions on Geoscience and Remote Sensing*, *41*(2), 253-264.

Betts, A. K., and Harshvardhan (1987), THERMODYNAMIC CONSTRAINT ON THE CLOUD LIQUID WATER FEEDBACK IN CLIMATE MODELS, *Journal of Geophysical Research-Atmospheres*, *92*(D7), 8483-8485.

Blossey, P. N., C. S. Bretherton, M. H. Zhang, A. N. Cheng, S. Endo, T. Heus, Y. G. Liu, A. P. Lock, S. R. de Roode, and K. M. Xu (2013), Marine low cloud sensitivity to an idealized climate change: The CGILS LES intercomparison, *J. Adv. Model. Earth Syst.*, *5*(2), 234-258.

Bodas-Salcedo, A., et al. (2011), COSP: Satellite simulation software for model assessment, *Bulletin of the American Meteorological Society*, *92*(8), 1023-1043.

Bony, S., et al. (2006), How well do we understand and evaluate climate change feedback processes?, *Journal of Climate*, *19*(15), 3445-3482.

Bretherton, C. S., and P. N. Blossey (2014), Low cloud reduction in a greenhouse-warmed climate: Results from Lagrangian LES of a subtropical marine cloudiness transition, *J. Adv. Model. Earth Syst.*, *6*(1), 91-114.

Bretherton, C. S., P. N. Blossey, and C. R. Jones (2013), Mechanisms of marine low cloud sensitivity to idealized climate perturbations: A single-LES exploration extending the CGILS cases, *J. Adv. Model. Earth Syst.*, *5*(2), 316-337.

Brient, F., and S. Bony (2013), Interpretation of the positive low-cloud feedback predicted by a climate model under global warming, *Climate Dynamics*, *40*(9-10), 2415-2431.

Caldwell, P. M., Y. Y. Zhang, and S. A. Klein (2013), CMIP3 Subtropical Stratocumulus Cloud Feedback Interpreted through a Mixed-Layer Model, *Journal of Climate*, *26*(5), 1607-1625.

Clement, A. C., R. Burgman, and J. R. Norris (2009), Observational and Model Evidence for Positive Low-Level Cloud Feedback, *Science*, *325*(5939), 460-464.

de Roode, S. R., A. P. Siebesma, S. dal Gesso, H. J. J. Jonker, J. Schalkwijk, and J. Sival (2014), A mixed-layer model study of the stratocumulus response to changes in large-scale conditions, *J. Adv. Model. Earth Syst.*, n/a-n/a.

Dee, D. P., et al. (2011), The ERA-Interim reanalysis: configuration and performance of the data assimilation system, *Quarterly Journal of the Royal Meteorological Society*, *137*(656), 553-597.

Eastman, R., and R. Wood (2015), Factors leading to the breakup of marine stratocumulus: a Lagrangian perspective using the A-Train satellites, *Journal of Climate*.

Eastman, R., S. G. Warren, and C. J. Hahn (2011), Variations in Cloud Cover and Cloud Types over the Ocean from Surface Observations, 1954–2008, *Journal of Climate*, *24*(22), 5914-5934.

Garcia, D. (2010), Robust smoothing of gridded data in one and higher dimensions with missing values, *Computational Statistics & Data Analysis*, *54*(4), 1167-1178.

Hartmann, D. L., and D. A. Short (1980), On the Use of Earth Radiation Budget Statistics for Studies of Clouds and Climate, *Journal of the Atmospheric Sciences*, *37*(6), 1233-1250.

Held, I. M., and B. J. Soden (2000), Water vapor feedback and global warming, *Annu. Rev. Energ. Environ.*, *25*, 441-475.

Klein, S. A., and D. L. Hartmann (1993), THE SEASONAL CYCLE OF LOW STRATIFORM CLOUDS, *Journal of Climate*, *6*(8), 1587-1606.

Klein, S. A., D. L. Hartmann, and J. R. Norris (1995), On the Relationships among Low-Cloud Structure, Sea Surface Temperature, and Atmospheric Circulation in the Summertime Northeast Pacific, *Journal of Climate*, *8*(5), 1140-1155.

Koshiro, T., and M. Shiotani (2014), Relationship between Low Stratiform Cloud Amount and Estimated Inversion Strength in the Lower Troposphere over the Global Ocean in Terms of Cloud Types, *Journal of the Meteorological Society of Japan*, *92*(1), 107-120.

Kubar, T. L., D. E. Waliser, J. L. Li, and X. Jiang (2012), On the Annual Cycle, Variability, and Correlations of Oceanic Low-Topped Clouds with Large-Scale Circulation Using Aqua MODIS and ERA-Interim, *Journal of Climate*, *25*(18), 6152-6174.

Li, J., J. Huang, K. Stamnes, T. Wang, Q. Lv, and H. Jin (2015), A global survey of cloud overlap based on CALIPSO and CloudSat measurements, *Atmospheric Chemistry and Physics*, *15*(1), 519-536.

Maddux, B. C., S. A. Ackerman, and S. Platnick (2010), Viewing Geometry Dependencies in MODIS Cloud Products, *Journal of Atmospheric and Oceanic Technology*, *27*(9), 1519-1528.

McCoy, D. T., D. L. Hartmann, and D. P. Grosvenor (2014), Observed Southern Ocean Cloud Properties and Shortwave Reflection. Part I: Calculation of SW

Flux from Observed Cloud Properties, *Journal of Climate*, *27*(23), 8836-8857.

Myers, T. A., and J. R. Norris (2013), Observational Evidence That Enhanced Subsidence Reduces Subtropical Marine Boundary Layer Cloudiness, *Journal of Climate*, *26*(19), 7507-7524.

Myers, T. A., and J. R. Norris (2014), On the Relationships between Subtropical Clouds and Meteorology in Observations and CMIP3 and CMIP5 Models, *Journal of Climate*, *28*(8), 2945-2967.

Nakajima, T., A. Higurashi, K. Kawamoto, and J. E. Penner (2001), A possible correlation between satellite-derived cloud and aerosol microphysical parameters, *Geophys. Res. Lett.*, *28*(7), 1171-1174.

Norris, J. R., and C. B. Leovy (1994), Interannual Variability in Stratiform Cloudiness and Sea Surface Temperature, *Journal of Climate*, *7*, 1915-1925.

Oreopoulos, L. (2005), The impact of subsampling on MODIS level-3 statistics of cloud optical thickness and effective radius, *Geoscience and Remote Sensing, IEEE Transactions on*, *43*(2), 366-373.

Platnick, S., M. D. King, S. A. Ackerman, W. P. Menzel, B. A. Baum, J. C. Riedi, and R. A. Frey (2003), The MODIS cloud products: Algorithms and examples from Terra, *Ieee Transactions on Geoscience and Remote Sensing*, *41*(2), 459-473.

Qu, X., A. Hall, S. Klein, and P. Caldwell (2014a), On the spread of changes in marine low cloud cover in climate model simulations of the 21st century, *Climate Dynamics*, *42*(9-10), 2603-2626.

Qu, X., A. Hall, S. Klein, and P. Caldwell (2014b), The strength of the tropical inversion and its response to climate change in 18 CMIP5 models, *Climate Dynamics*, 1-22.

Qu, X., A. Hall, S. A. Klein, DeAngelis, and M. Anthony (2015), Positive tropical marine low-cloud cover feedback inferred from cloud-controlling factors, *Geophys. Res. Lett.*, n/a-n/a.

Quaas, J. (2012), Evaluating the "critical relative humidity" as a measure of subgrid-scale variability of humidity in general circulation model cloud cover parameterizations using satellite data, *Journal of Geophysical Research: Atmospheres*, *117*(D9), n/a-n/a.

Randall, D. A. (1984), Stratocumulus cloud deepening through entrainment, *Tellus A*, *36A*(5), 446-457.

Richter, I., and S.-P. Xie (2008), Muted precipitation increase in global warming simulations: A surface evaporation perspective, *Journal of Geophysical Research: Atmospheres*, *113*(D24), n/a-n/a.

Rieck, M., L. Nuijens, and B. Stevens (2012), Marine Boundary Layer Cloud Feedbacks in a Constant Relative Humidity Atmosphere, *Journal of the Atmospheric Sciences*, *69*(8), 2538-2550.

Schneider, S. H. (1972), Cloudiness as a Global Climatic Feedback Mechanism: The Effects on the Radiation Balance and Surface Temperature of Variations in Cloudiness, *Journal of the Atmospheric Sciences*, *29*(8), 1413-1422.

Schreier, M. M., B. H. Kahn, K. Sušelj, J. Karlsson, S. C. Ou, Q. Yue, and S. L. Nasiri (2014), Atmospheric parameters in a subtropical cloud regime transition

derived by AIRS and MODIS: observed statistical variability compared to ERA-Interim, *Atmos. Chem. Phys.*, *14*(7), 3573-3587.

Sherwood, S. C., S. Bony, and J.-L. Dufresne (2014), Spread in model climate sensitivity traced to atmospheric convective mixing, *Nature*, *505*(7481), 37-42.

Tsushima, Y., S. Emori, T. Ogura, M. Kimoto, M. J. Webb, K. D. Williams, M. A. Ringer, B. J. Soden, B. Li, and N. Andronova (2006), Importance of the mixed-phase cloud distribution in the control climate for assessing the response of clouds to carbon dioxide increase: a multi-model study, *Climate Dynamics*, *27*(2-3), 113-126.

van der Dussen, J. J. (2014), An LES model study of the influence of the free troposphere on the stratocumulus response to a climate perturbation.

van der Dussen, J. J., S. R. de Roode, and A. P. Siebesma (2013), Factors Controlling Rapid Stratocumulus Cloud Thinning, *Journal of the Atmospheric Sciences*, *71*(2), 655-664.

van der Dussen, J. J., S. R. de Roode, S. D. Gesso, and A. P. Siebesma (2015), An LES model study of the influence of the free tropospheric thermodynamic conditions on the stratocumulus response to a climate perturbation, *J. Adv. Model. Earth Syst.*, *7*(2), 670-691.

Vial, J., J. L. Dufresne, and S. Bony (2013), On the interpretation of inter-model spread in CMIP5 climate sensitivity estimates, *Climate Dynamics*, *41*(11-12), 3339-3362.

Wang, G. J., D. Garcia, Y. Liu, R. de Jeu, and A. J. Dolman (2012), A three-dimensional gap filling method for large geophysical datasets: Application to global

satellite soil moisture observations, *Environmental Modelling & Software*, *30*, 139-142.

Webb, M. J., F. Lambert, and J. M. Gregory (2013), Origins of differences in climate sensitivity, forcing and feedback in climate models, *Climate Dynamics*, *40*(3-4), 677-707.

Webb, M. J., et al. (2006), On the contribution of local feedback mechanisms to the range of climate sensitivity in two GCM ensembles, *Climate Dynamics*, *27*(1), 17-38.

Wood, R. (2007), Cancellation of Aerosol Indirect Effects in Marine Stratocumulus through Cloud Thinning, *Journal of the Atmospheric Sciences*, *64*(7), 2657-2669.

Wood, R. (2012), Stratocumulus Clouds, *Monthly Weather Review*, *140*(8), 2373-2423.

Wood, R., and C. S. Bretherton (2006), On the relationship between stratiform low cloud cover and lower-tropospheric stability, *Journal of Climate*, *19*(24), 6425-6432.

Yue, Q., B. H. Kahn, H. Xiao, M. M. Schreier, E. J. Fetzer, J. Teixeira, and K. Sušelj (2013), Transitions of cloud-topped marine boundary layers characterized by AIRS, MODIS, and a large eddy simulation model, *Journal of Geophysical Research: Atmospheres*, *118*(15), 8598-8611.

Zelinka, M. D., S. A. Klein, and D. L. Hartmann (2012), Computing and Partitioning Cloud Feedbacks Using Cloud Property Histograms. Part II: Attribution to Changes in Cloud Amount, Altitude, and Optical Depth, *Journal of Climate*, *25*(11), 3736-3754.

Zelinka, M. D., S. A. Klein, K. E. Taylor, T. Andrews, M. J. Webb, J. M. Gregory, and P. M. Forster (2013), Contributions of Different Cloud Types to Feedbacks and Rapid Adjustments in CMIP5*, *Journal of Climate*, *26*(14), 5007-5027.

Zieger, S., A. V. Babanin, and I. R. Young (2014), Changes in ocean surface wind with a focus on trends in regional and monthly mean values, *Deep Sea Research Part I: Oceanographic Research Papers*, *86*(0), 56-67.

Tables

	8-DAY	1-DAY
U10m	ERA-Interim octet-averaged 10 meter wind speed	ERA-Interim 10 meter wind speed interpolated to the MODIS overpass time
SST	ERA-Interim octet-averaged sea-surface temperature	ERA-Interim skin temperature over oceans interpolated to the MODIS overpass time
RHFT	AIRS RH octet-averaged and averaged 450-650 hPa	ERA-Interim RH averaged 450-650 hPa and interpolated to the MODIS overpass time
EIS	EIS Calculated according to *Wood and Bretherton* [2006] using AIRS retrievals of thermodynamic properties	EIS calculated using ERA-Interim data (interpolated to the MODIS overpass time) according to *Wood and Bretherton* [2006]
ω550	Subsidence at 550 hPa octet-averaged from ERA-Iterim	ERA-Interim subsidence at 550 hPa interpolated to the MODIS overpass time
LCC	MODIS Collection 6 8-Day CTP histogram for solar zenith angle less than 32°	MODIS Collection 5.1 cloud fraction for liquid-topped and single-layer cloud scenes only

Table 1 Summary of the remote sensing and reanalysis data used in this study.

Compositing variables	Assumed changes in a warmed climate	R^2LUT 8-Day	R^2LUT 1-Day	R^2ML 8-Day	R^2ML 1-Day
EIS	+0.2K [*Webb et al*., 2013]	0.56	0.49	0.54	0.5
U10m	Assumed constant				
SST	+1K				
RHFT	CMIP5 change between historical and RCP85 normalized by local change in SST [see text]				
ω550	CMIP5 change between historical and RCP85 normalized by local change in SST [see text]				

Table 2 Summary of the set of compositing variables used in this paper to predict low cloud cover and assumed changes with warming. The explained variance in the observed record of LCC between 40°S-40°N at monthly-mean and 4°x4° resolution is shown in the right 4 columns. LUT indicates that the composite was used as a look up table to predict LCC. ML indicates that the coefficients from the multiple linear regression were used to predict LCC.

	1-Day			8-Day		
	40°S-40°N	TradeCu	Sc	40°S-40°N	TradeCu	Sc
EIS	9.5±1.6	8.3±2.4	10.6±4.0	4.2±2.5	2.7±2.4	2.0±2.4
U10m	6.0±1.5	7.2±1.9	7.2±3.4	3.6±1.1	3.8±1.5	4.5±3.0
SST	-2.7±8.5	-5.9±8.4	5.5±18.0	-8.6±3.5	-8.0±2.7	-0.9±10.3
RHFT	5.6±1.9	5.3±2.2	3.2±3.2	2.4±1.5	1.2±1.7	2.8±3.1
ω550	-2.3±0.8	-2.3±1.2	-1.4±1.9	-0.5±0.9	-1.0±0.9	1.3±2.4

Table 3 Coefficients relating LCC to each control variable in each region and data set. The left three columns show the coefficients from the 1-Day data set, the right three show the 8-Day data set. For each data set mean coefficients for each region from Figure 1 are shown with the standard deviation over all estimates of the coefficient. Note that the 40°S-40°N region has sixteen estimates for each coefficient, while the stratocumulus (Sc), and trade cumulus (TradeCu) regions have twenty.

Figure Captions List

Figure 1 The mean LCC from the (a) 1-Day and (b) 8-Day data sets. Compositing is performed on each three-month season independently and in each of the 20° latitude bands (noted on the latitude axis), each of the stratocumulus regions [*Klein and Hartmann*, 1993] (shown in pink), and each of the subtropical trade cumulus regimes (shown in purple).

Figure 2 The correlations between the predictor variables considered in this study for (a) the 1-Day data set, and (b) the 8-Day data set. All data is taken from the region 40°S-40°N over all seasons and at the native temporal resolution of each data set.

Figure 3 The regression coefficients from each compositing analysis weighted by the standard deviations over space and time of each variable in the 40°S-40°N region. The median, spread, and outliers describing all the estimates of each coefficient within each region and for each dataset are shown in the figure. The regression coefficients for each variable are shown for the 1-Day (shown as red, blue, and green) and 8-Day (shown as yellow, teal, and orange) data set. Compositing is performed independently on each season and geographic region. This yields estimates of each of the coefficients. Three regions are considered: 40°S-40°N split into 20° latitude bands (*All* in the legend), the stratocumulus regimes (*Sc*), and the trade cumulus regions (*TradeCu*) (regions are shown in Figure 1). This yields sixteen estimates of each coefficient for the 40°S-40°N region, twenty for the stratocumulus regions, and twenty for the trade cumulus regions.

Figure 4 as in Figure 3, but using near surface air temperature and RH instead of SST and U10m. Near surface air temperature and RH from AIRS are used in the 8-Day data set. 1000 hPa air temperature and RH from ECMWF-interim are used in the 1-Day data set.

Figure 5 Correlation coefficients between the predicted LCC and observational records of LCC. All data has been averaged to monthly 4°x4° resolution before calculating the correlation coefficient. The left column shows the results for the 1-Day data set and the right column shows the results for the 8-Day data set. The LCC is predicted using the mean of the 16 composites from the 20° latitude bands and four seasons combined with the observational record of each control variable. Two different prediction methods are shown. The top two rows show the correlation coefficient for LCC predicted by utilizing the coefficients of the mean composite and the observational record of each variable. The bottom two rows show the LCC predicted by using the mean composite as a look up table for LCC combined with the observational record of each control variable. Anomalies in LCC are calculated by subtracting the climatological seasonal cycle. The correlation between the observed and predicted anomalies in LCC are shown in the top row (using the coefficients from the multiple linear regression) and third row (using the look up table). If the correlation coefficient is significant at 95% confidence the grid cell is marked with a dot.

Figure 6 The variance in LCC contributed by each control variable to LCC scaled by the total predicted variance in LCC. The variance is calculated using the coefficients yielded by performing multiple linear regression on the mean composite and the observed control

variables. The left column shows results from the 1-Day data set and the right column shows results from the 8-Day data set. Each row is for a different control variable and is noted on the right.

Figure 7 The change in percent cloud cover in GCMs and the change in percent LCC inferred from observations. (a) The mean change in cloud fraction across 30 models in the CMIP5 archive. (b) the model with the most positive change in cloud fraction (bcc-csm1-1-m). (c) the model with the most negative change in cloud fraction (IPSL-CM5A-LR). (d-g) the change in LCC inferred from the observations assuming SST increases by 1K, EIS increases by 0.2K, RHFT changes consistent with the multi-model change in RHFT predicted by CMIP5, ω550 changes consistent with the multi-model mean change in ω550 in CMIP5. (d-e) The change inferred from the composite created from the 40°S-40°N data. (f-g) the change inferred from the data within the trade cumulus regions (see Figure 1). (d) and (f) inferred from the 1-Day data set. (e) and (g) inferred from the 8-Day data set.

Figure 8 The zonal-mean change in LCC inferred from the observations from AIRS, MODIS, and ERA-interim as compared to the CMIP5 change in total cloud fraction (CF) from 30 models and scaled by the change in SST between the historical and RCP8.5 experiments. The multi-model mean change in CF from CMIP5 is shown as a dark dashed line, with a standard deviation across all the models shown as a hatched area, and the outliers shown as a light dashed line. The change in LCC inferred from observations is shown using colored lines. The change in LCC inferred from the composites of the 1-

Day and 8-Day data sets and the entire 40°S-40°N region and trade-cumulus regions are distinguished by different markers (see legend). The changes in LCC inferred from observations due to an increase in SST of 1K, EIS increasing by 0.2K, and CMIP5 predicted changes in RHFT and ω550 are shown as a black line. The components of this total change are also shown individually to show the relative dominance of the temperature contribution. The change inferred from only the 1K SST increase is shown in blue; the change from the 0.2K EIS increase is shown in red; the change inferred due to subsidence changes is shown in purple; and the change inferred due to changes in free tropospheric RH is shown in dark red.

Figures

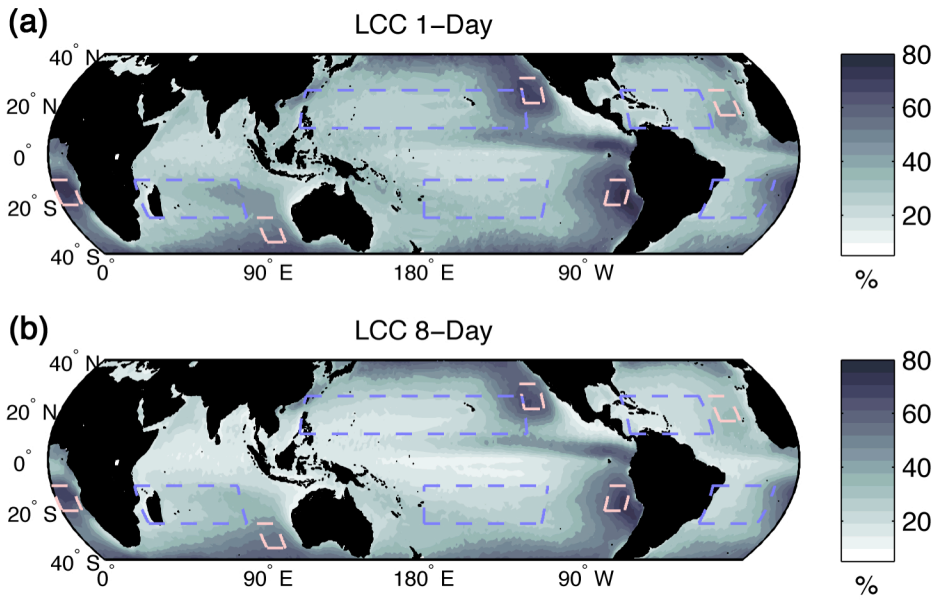

Figure 1 The mean LCC from the (a) 1-Day and (b) 8-Day data sets. Compositing is performed on each three-month season independently and in each of the 20° latitude bands (noted on the latitude axis), each of the stratocumulus regions [*Klein and Hartmann*, 1993] (shown in pink), and each of the subtropical trade cumulus regimes (shown in purple).

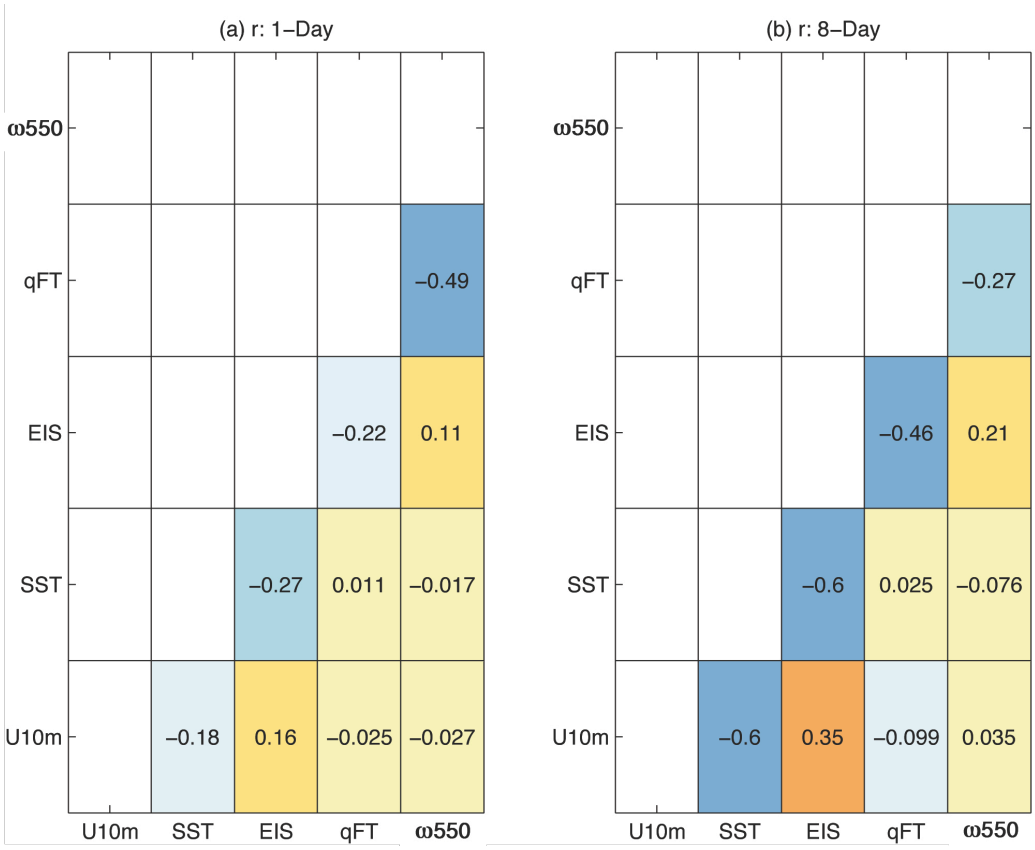

Figure 2 The correlations between the predictor variables considered in this study for (a) the 1-Day data set, and (b) the 8-Day data set. All data is taken from the region 40°S-40°N over all seasons and at the native temporal resolution of each data set.

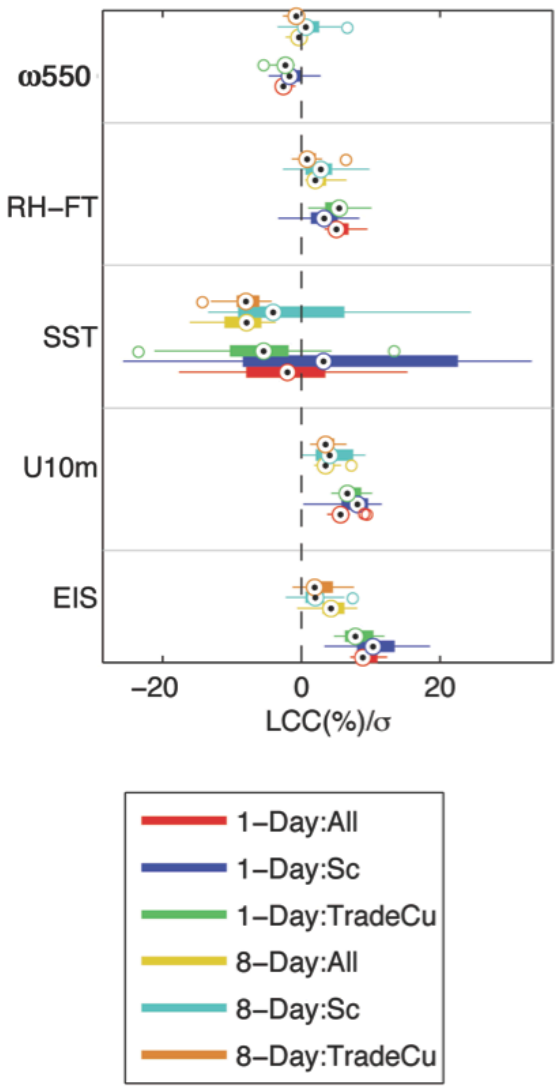

Figure 3 The regression coefficients from each compositing analysis weighted by the standard deviations over space and time of each variable in the 40°S-40°N region. The median, spread, and outliers describing all the estimates of each coefficient within each region and for each dataset are shown in the figure. The regression coefficients for each variable are shown for the 1-Day (shown as red, blue, and green) and 8-Day (shown as yellow, teal, and orange) data set. Compositing is performed independently on each season and geographic region. This yields estimates of each of the coefficients. Three regions are considered: 40°S-40°N split into 20° latitude bands (*All* in the legend), the stratocumulus regimes (*Sc*), and the trade cumulus regions (*TradeCu*) (regions are shown in Figure 1). This yields sixteen estimates of each coefficient for the 40°S-40°N region, twenty for the stratocumulus regions, and twenty for the trade cumulus regions.

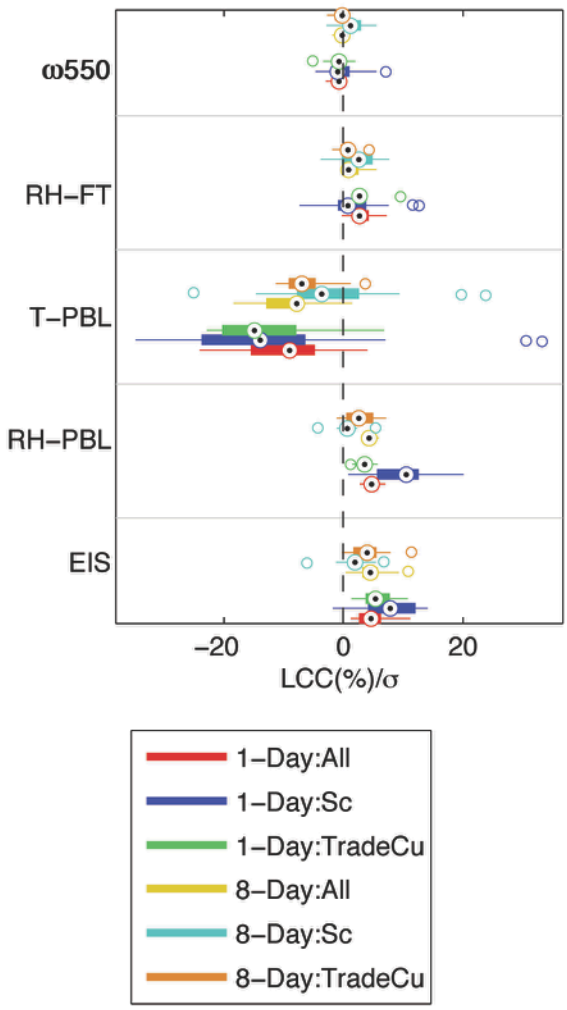

Figure 4 as in Figure 3, but using near surface air temperature and RH instead of SST and U10m. Near surface air temperature and RH from AIRS are used in the 8-Day data set. 1000 hPa air temperature and RH from ECMWF-interim are used in the 1-Day data set.

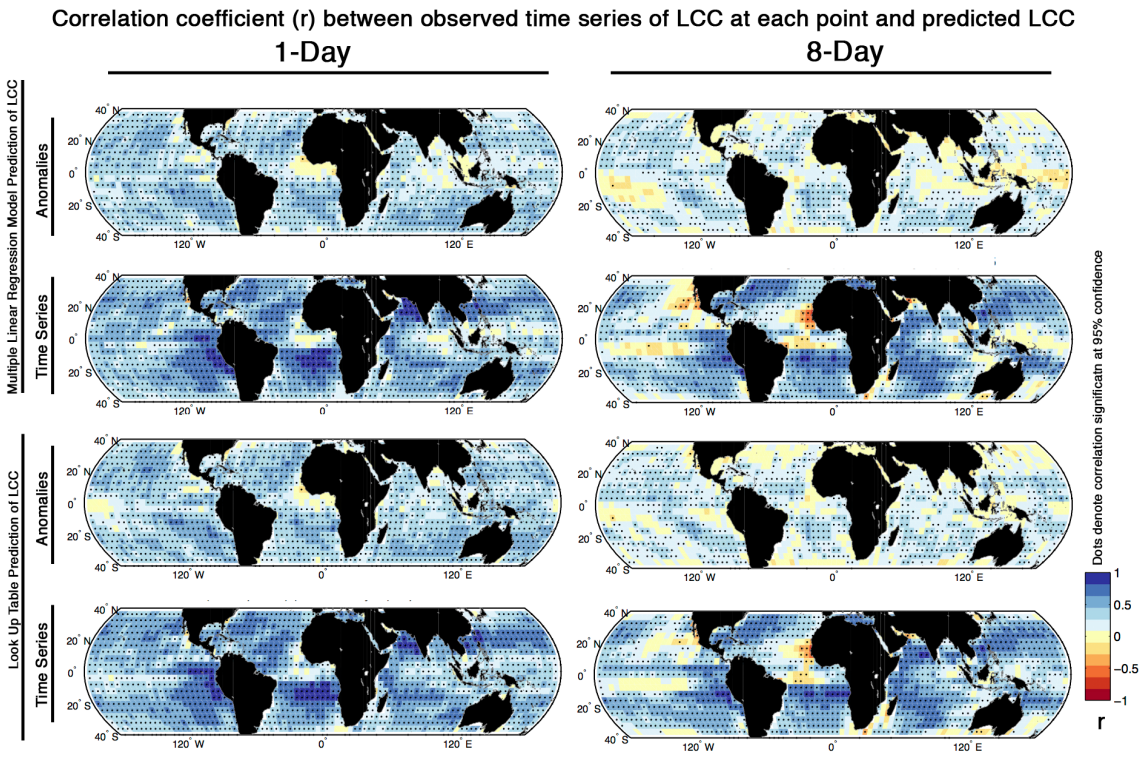

Figure 5 Correlation coefficients between the predicted LCC and observational records of LCC. All data has been averaged to monthly 4°x4° resolution before calculating the correlation coefficient. The left column shows the results for the 1-Day data set and the right column shows the results for the 8-Day data set. The LCC is predicted using the mean of the 16 composites from the 20° latitude bands and four seasons combined with the observational record of each control variable. Two different prediction methods are shown. The top two rows show the correlation coefficient for LCC predicted by utilizing the coefficients of the mean composite and the observational record of each variable. The bottom two rows show the LCC predicted by using the mean composite as a look up table for LCC combined with the observational record of each control variable. Anomalies in LCC are calculated by subtracting the climatological seasonal cycle. The correlation between the observed and predicted anomalies in LCC are shown in the top row (using the coefficients from the multiple linear regression) and third row (using the look up table). If the correlation coefficient is significant at 95% confidence the grid cell is marked with a dot.

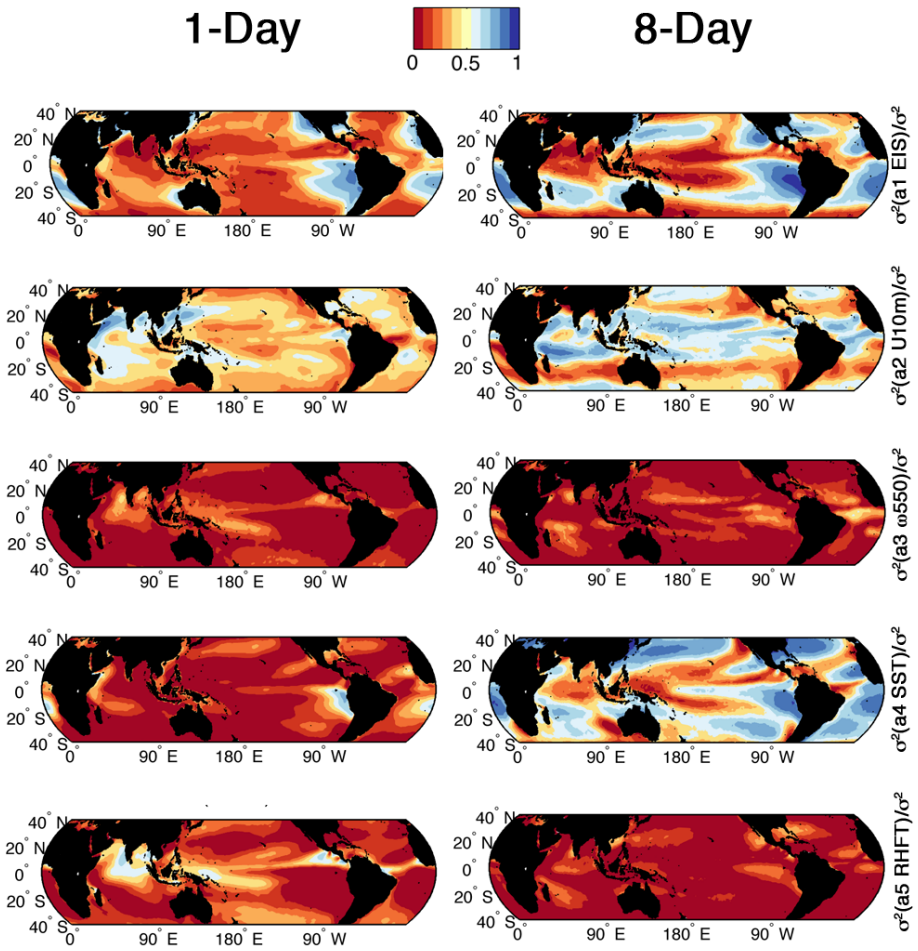

Figure 6 The variance in LCC contributed by each control variable to LCC scaled by the total predicted variance in LCC. The variance is calculated using the coefficients yielded by performing multiple linear regression on the mean composite and the observed control variables. The left column shows results from the 1-Day data set and the right column shows results from the 8-Day data set. Each row is for a different control variable and is noted on the right.

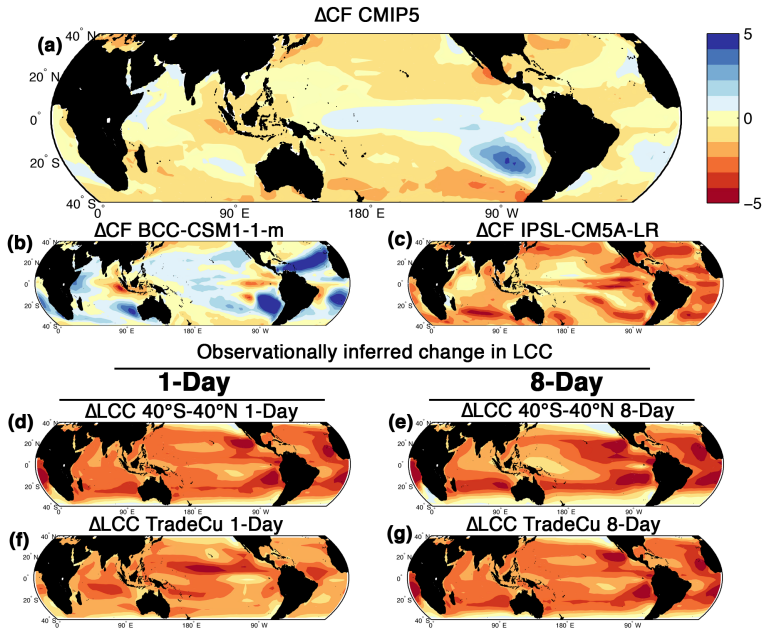

Figure 7 The change in percent cloud cover in GCMs and the change in percent LCC inferred from observations. (a) The mean change in cloud fraction across 30 models in the CMIP5 archive. (b) the model with the most positive change in cloud fraction (bcc-csm1-1-m). (c) the model with the most negative change in cloud fraction (IPSL-CM5A-LR). (d-g) the change in LCC inferred from the observations assuming SST increases by 1K, EIS increases by 0.2K, RHFT changes consistent with the multi-model change in RHFT predicted by CMIP5, ω550 changes consistent with the multi-model mean change in ω550 in CMIP5. (d-e) The change inferred from the composite created from the 40°S-40°N data. (f-g) the change inferred from the data within the trade cumulus regions (see Figure 1). (d) and (f) inferred from the 1-Day data set. (e) and (g) inferred from the 8-Day data set.

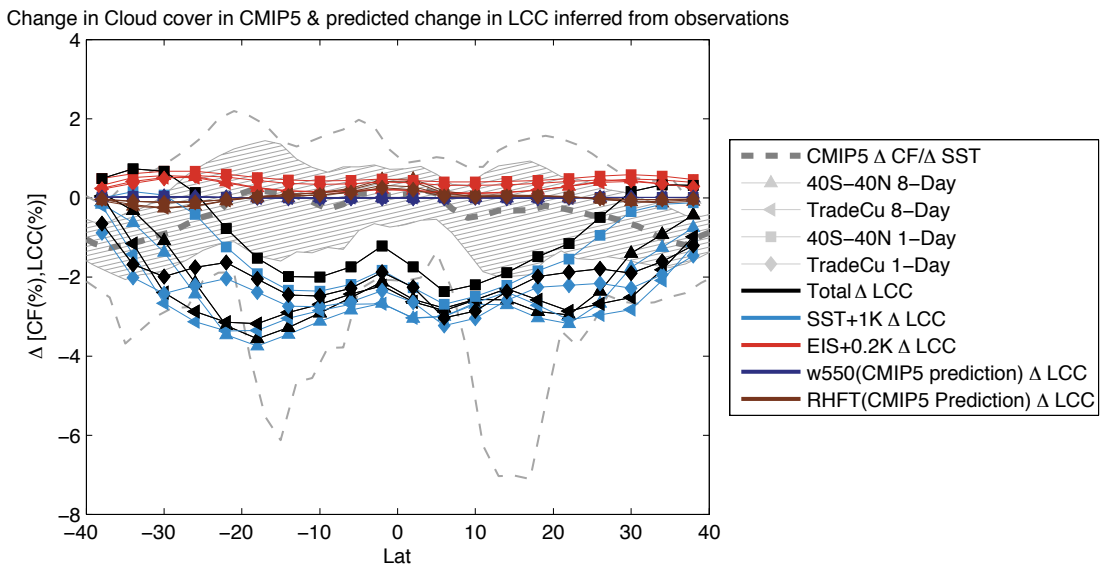

Figure 8 The zonal-mean change in LCC inferred from the observations from AIRS, MODIS, and ERA-interim as compared to the CMIP5 change in total cloud fraction (CF) from 30 models and scaled by the change in SST between the historical and RCP8.5 experiments. The multi-model mean change in CF from CMIP5 is shown as a dark dashed line, with a standard deviation across all the models shown as a hatched area, and the outliers shown as a light dashed line. The change in LCC inferred from observations is shown using colored lines. The change in LCC inferred from the composites of the 1-Day and 8-Day data sets and the entire 40°S-40°N region and trade-cumulus regions are distinguished by different markers (see legend). The changes in LCC inferred from observations due to an increase in SST of 1K, EIS increasing by 0.2K, and CMIP5 predicted changes in RHFT and ω550 are shown as a black line. The components of this total change are also shown individually to show the relative dominance of the temperature contribution. The change inferred from only the 1K SST increase is shown in blue; the change from the 0.2K EIS increase is shown in red; the change inferred due to subsidence changes is shown in purple; and the change inferred due to changes in free tropospheric RH is shown in dark red.